Supplementary Information

Restoration of Li^+ Pathways in the [010] Direction during Direct Regeneration for Spent $LiFePO_4$

Shuaipeng Hao[a], Yuelin Lv[a], Yi Zhang[a], Shuaiwei Liu[b], Zhouliang Tan[c], Wei Liu[d,e], Yuanguang Xia[d,e], Wen Yin[d,e], Yaqi Liao[a], Haijin Ji[a], Yuelin Kong[a], Yudi Shao[a], Yunhui Huang[a]*, Lixia Yuan[a]*

[a] State Key Laboratory of Material Processing and Die & Mould Technology, School of Materials Science and Engineering, Huazhong University of Science and Technology, Wuhan, Hubei, 430074, China.

[b] Karlsruhe Institute of Technology (KIT), Institute for Applied Materials-Energy Storage Systems (IAM-ESS), Hermann-von-Helmholtz-Platz 1, D-76344 Eggenstein-Leopoldshafen, Karlsruhe, Germany.

[c] State Key Laboratory of Chemistry and Utilization of Carbon Based Energy Resources, College of Chemistry, Xinjiang University, Urumqi, 830017, Xinjiang, China

[d] Institute of High Energy Physics Chinese Academy of Sciences, Beijing, 100049, P. R. China.

[e] China Spallation Neutron Source Science Center, Dongguan, 523803, P. R. China.

E-mail: huangyh@hust.edu.cn；yuanlixia@hust.edu.cn

Methods

Battery Disassembly Separation

Spent $LiFePO_4$ and $LiNi_{0.5}Co_{0.2}Mn_{0.3}O_2$ pouch batteries were discharged by immersing them in 2 mol/L NaCl solution for 24 h. Then, the batteries were manually disassembled to separate the cathode electrode, anode electrode, aluminum-plastic film, and diaphragm. The stripped cathode electrode was cleaned with dimethyl carbonate (DMC).

Separation of Al foil and spent LFP/NCM523 cathode using TA solution

The spent LFP and spent NCM523 cathodes were immersed in a 1 mol/L TA solution with a solid-liquid ratio of 30 g/L at 25 °C where the Al foils were separated from the spent LFP layer and the spent NCM523 layer. Afterward, the Al foil was then removed from the solution, washed three times with deionized water, and dried at 80 °C for 6 h to obtain the separated aluminum foil. The TA solution and separated S-LFP cathode were used directly in the hydrothermal regeneration process.

Direct regeneration process

Firstly, the TA solution and separated spent LFP cathode from the separation step were transferred to the PTFE liner of a 50 mL autoclave. Then lithium hydroxide monohydrate ($LiOH{\cdot}H_2O$) was added, and the mixture was stirred for 30 minutes and subsequently reacted in an oven at different temperatures and times. The reactants were centrifugally washed three times with deionized water and the powder was gathered and dried in an oven at 80 °C for 6 h. Lastly, it was mixed with 2%wt. of Li_2CO_3 and annealed under argon atmosphere at different temperatures and times (heating rate 5 °C/min) to finally obtain the regenerated LFP.

Optimal conditions: The TA solution and separated spent LFP cathode (solid-liquid ratio of 30 g/L) from the separation step were transferred to the PTFE liner of a 50 mL autoclave. Then 2 mol/L $LiOH{\cdot}H_2O$ was put in and heated at 120 °C for 5 h. After

cooling to room temperature and centrifugal washing, H-LFP was obtained by drying. H-LFP was then mixed with 2%wt. Li_2CO_3 and annealed at 650 °C for 5 h to obtain R-LFP.

As comparison experiments, S2-LFP (30% degradation), S3-LFP (50% degradation) and S4-LFP (75% degradation) were regenerated according to the above regeneration process to obtain R2-LFP, R3-LFP and R4-LFP. Moreover, S-LFP was mixed with Li_2CO_3 at a molar ratio of Li/Fe of 1.02 for 5 h at 400 rpm/min, calcined at 350 °C for 2 h and then at 650 °C for 10 h to obtain RS-LFP.

Material characterizations

The XRD measurements were carried out on an Empyrean model instrument from Panacor in the Netherlands under the following conditions: radiation source Cu Kα (λ = 1.54184 Å), and a measuring range of 10-80°. H-LFP and R-LFP using an Ag Kα (λ= 0.55941 A). The in-situ XRD measurements used CR2025coin cells with a glass window (diameter=5 mm). The XRD data were characterized using and analyzed with HighScore Plus and GSAS II software. The elemental contents of the cathode materials and solutions were characterized by an inductively coupled plasma emission spectrometer (ICP-OES) from Leeman Labs, USA. The microstructure and morphology of the materials were analyzed by a Nova NanoSEM450 field emission scanning electron microscope (SEM) from FEI, USA and a Tecnai G2 20 transmission electron microscope (TEM) from FEI, Netherlands. The composition of the cathode material was characterized by a thermogravimetric thermal analyzer (TG) from NETZSCH Instruments Manufacturing GmbH, Germany. X-ray photoelectron spectroscopy (XPS) of AXIS-ULTRA DLD-600W from Shimadzu-Kratos, Japan was utilized to detect the variation of elements and valence states on the surface of the materials and combined with Avantage software for analysis. The variation of functional groups and bond lengths of materials was investigated by a LabRAM HR800 laser confocal Raman spectrometer (Raman) from Horiba JobinYvon and a Nicolet iS50R Fourier Transform Infrared Spectrometer (FT-IR) from Thermo Scientific, USA. The local structural

evolution of the material (atomic occupancy, bond lengths between atoms) was measured by the Multi-Physics Spectrometer (MPI) at the China Scattered Neutron Source (CNSNS) and combined with the GASA II software to analyze it.

Computational details

We have employed the Vienna Ab Initio Package (VASP) to perform the density functional theory (DFT) calculations within the generalized gradient approximation (GGA) using the PBE formulation. We have chosen the projected augmented wave (PAW) potentials to describe the ionic cores and take valence electrons into account using a plane wave basis set with a kinetic energy cutoff of 500 eV. Partial occupancies of the Kohn-Sham orbitals were allowed using the Gaussian smearing method with a width of 0.05 eV. The electronic energy was considered self-consistent when the energy change was smaller than 10-5 eV. A geometry optimization was considered convergent when the force change was smaller than 0.05 eV/Å. Grimme's DFT-D3 methodology was used to describe the dispersion interactions. During structural optimizations, the gamma point in the Brillouin zone was used for k-point sampling, and all atoms were allowed to relax. Finally, the nudged elastic band (NEB) method determined Li migration transition states for path steps. The NEB method discretizes the path between the reactant and product into a series of structural images.

Electrochemical tests

Cathode electrode powder, polyvinylidene fluoride (5wt% dissolved in N-methyl-2-pyrrolidone), and carbon black were blended in a weight ratio of 8:1:1 and stirred for 10 h. The slurry was covered with carbon-coated Al foil and dried in an oven at 80 °C for 6 h. Cycling performance was performed on assembled 2032-coin cells and $LiFePO_4$||Li pouch cells at 2.5-4.3 V (1 C=170 mA/g) using the Land and Neware battery test system. The electrolyte was 1.0 M $LiPF_6$ in EC: DEC=1:1 Vol% with 5.0% FEC. A Princeton electrochemical workstation measured cyclic voltammetry (CV) and electrochemical impedance spectroscopy (EIS). The Galvanostatic Intermittent

Titration Technique (GITT) was measured utilizing the Land Battery Test System with a pulse time of 10 min and a relaxation time of 40 min.

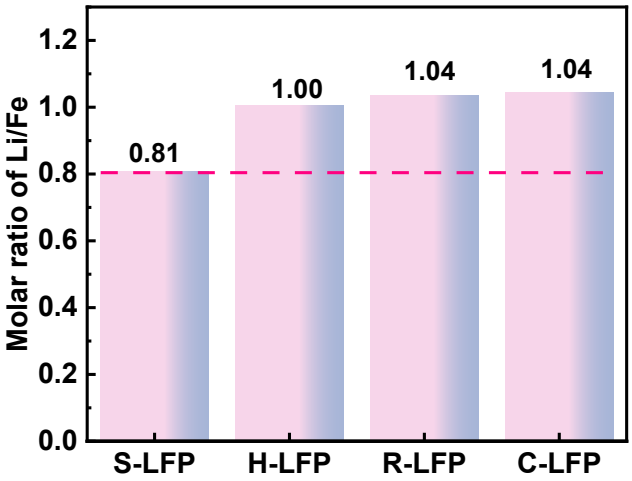

Fig. S1 Elemental analysis of S-LFP, H-LFP, R-LFP and C-LFP.

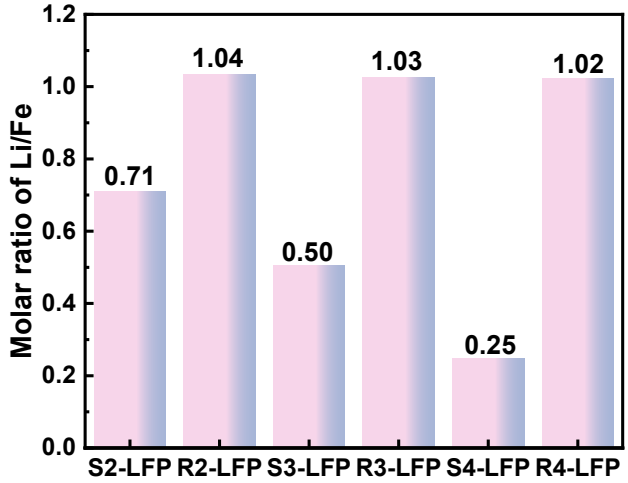

Fig. S2 Elemental analysis of S2-LFP, S3-LFP, S4-LFP, R2-LFP, R3-LFP and R4-LFP.

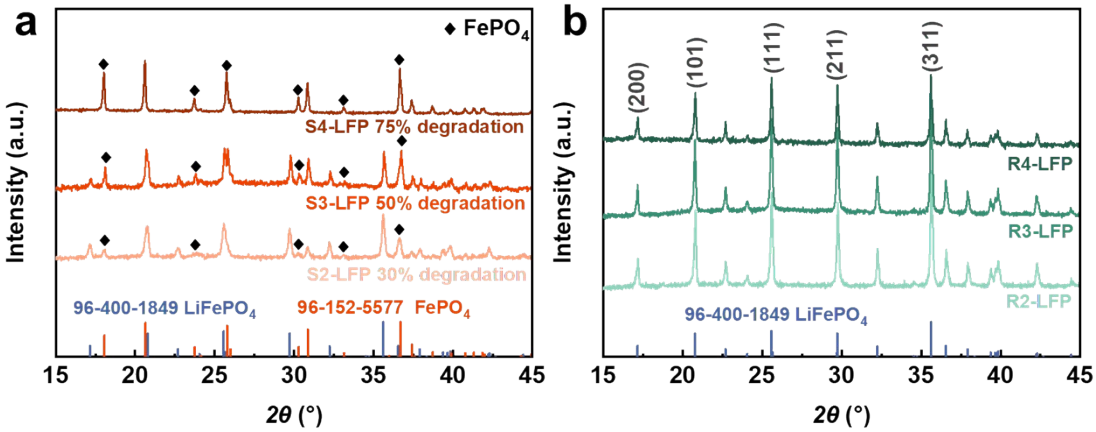

Fig. S3 XRD patterns of S2-LFP, S3-LFP, S4-LFP, R2-LFP, R3-LFP and R4-LFP.

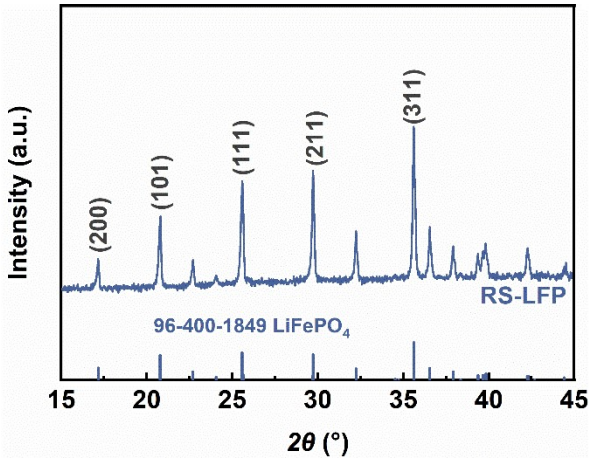

Fig. S4 XRD pattern of RS-LFP.

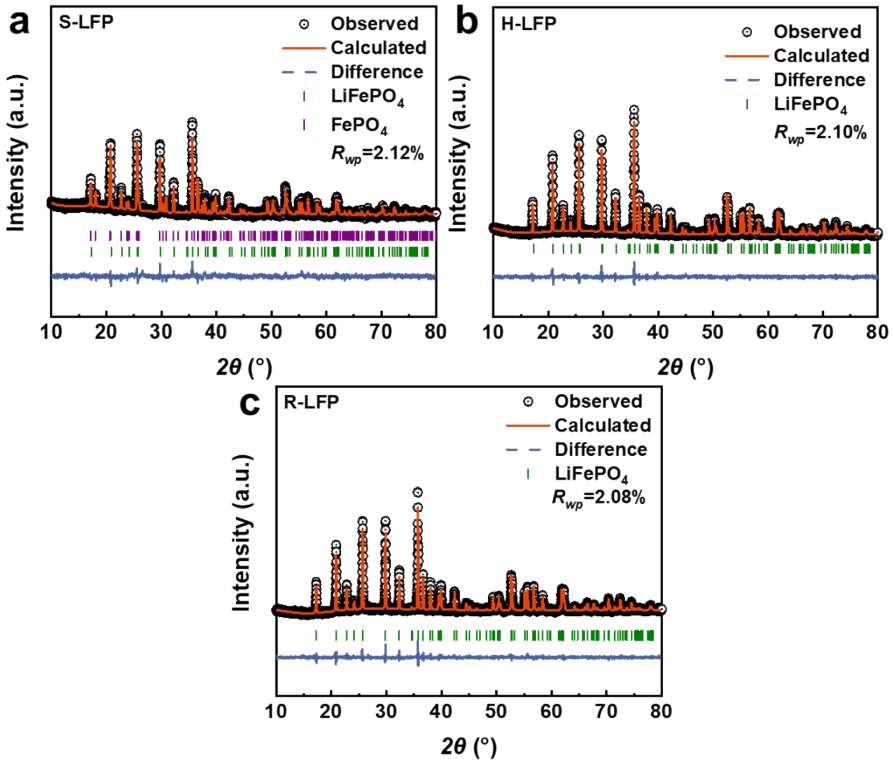

Fig. S5 Rietveld refinement of XRD patterns of S-LFP, H-LFP and R-LFP.

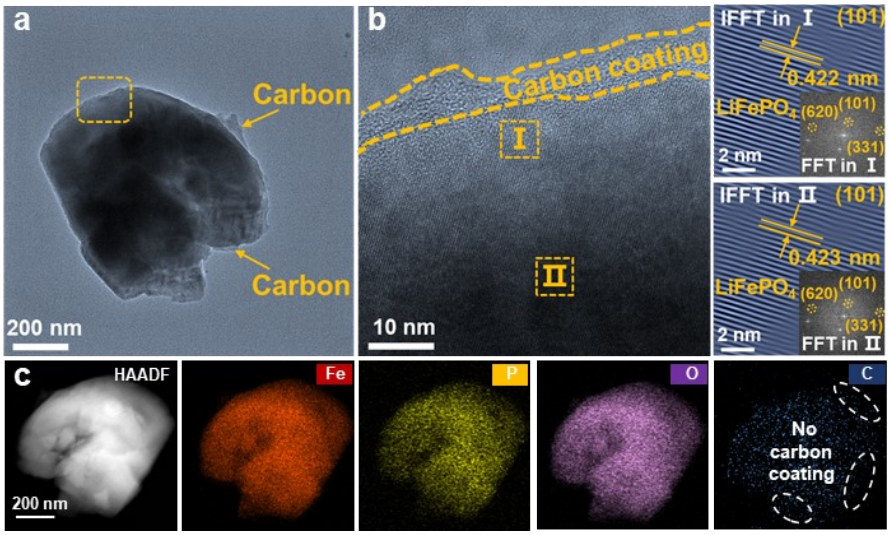

Fig. S6 (a, b) HRTEM images and enlarged images of H-LFP (IFFT and FFT images within the I-II region). (c) HAADF-STEM and EDS images of H-LFP.

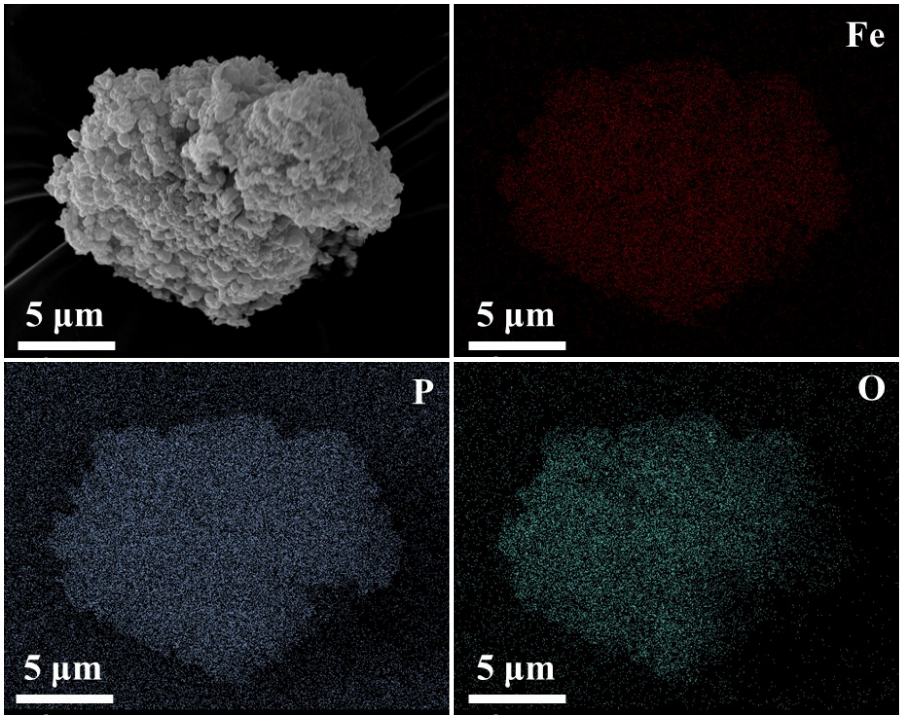

Fig. S7 EDS image of S-LFP (Fe, P and O elements).

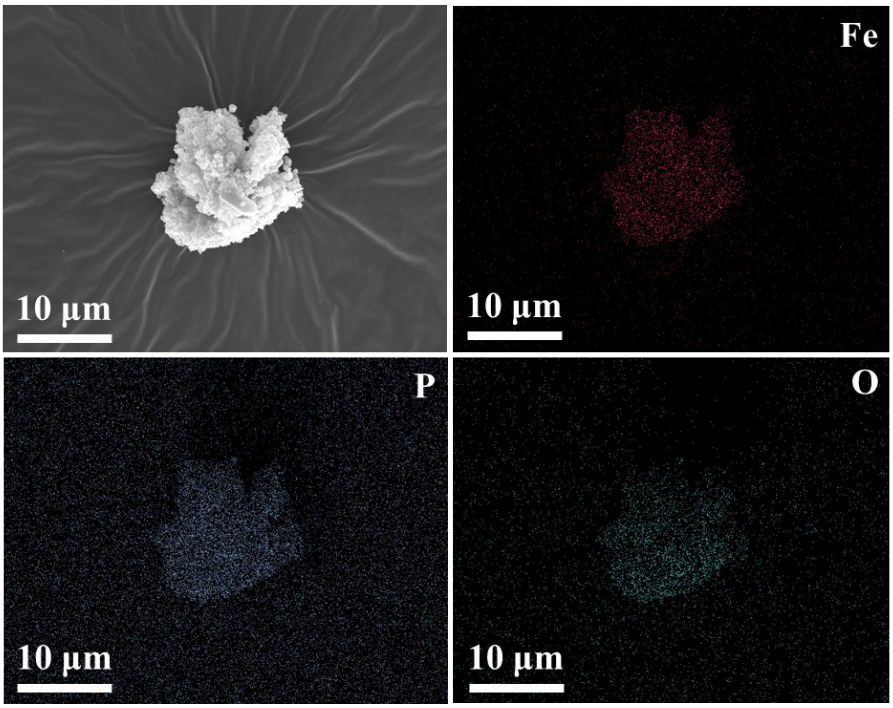

Fig. S8 EDS image of R-LFP (Fe, P and O elements).

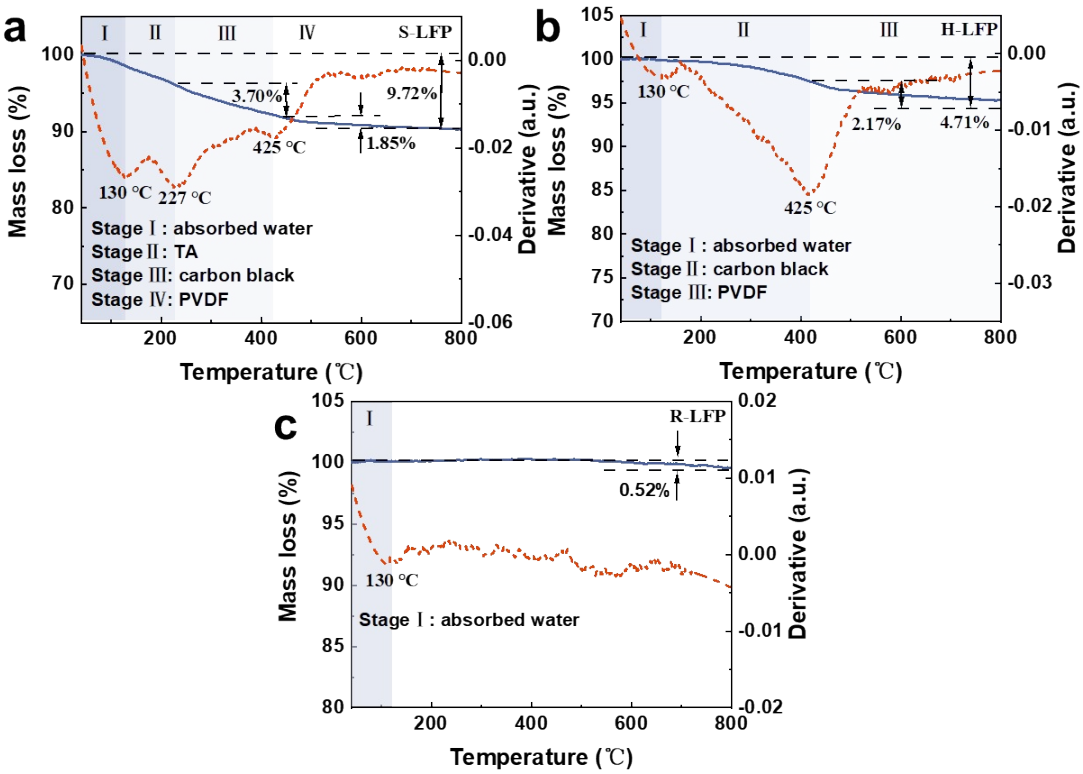

Fig. S9 TG curves of S-LFP, H-LFP and R-LFP from 40 to 800 °C

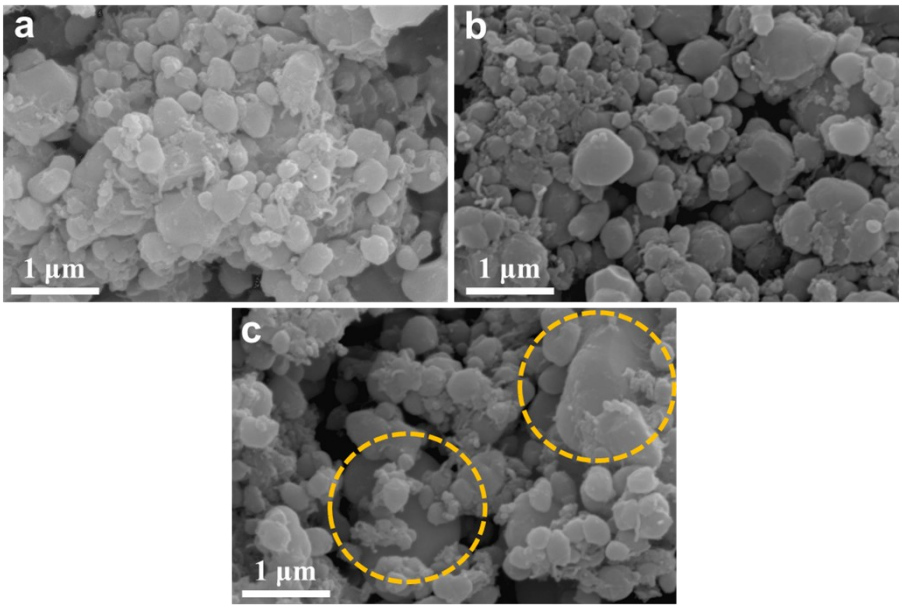

Fig. S10 SEM images of S-LFP, H-LFP and R-LFP.

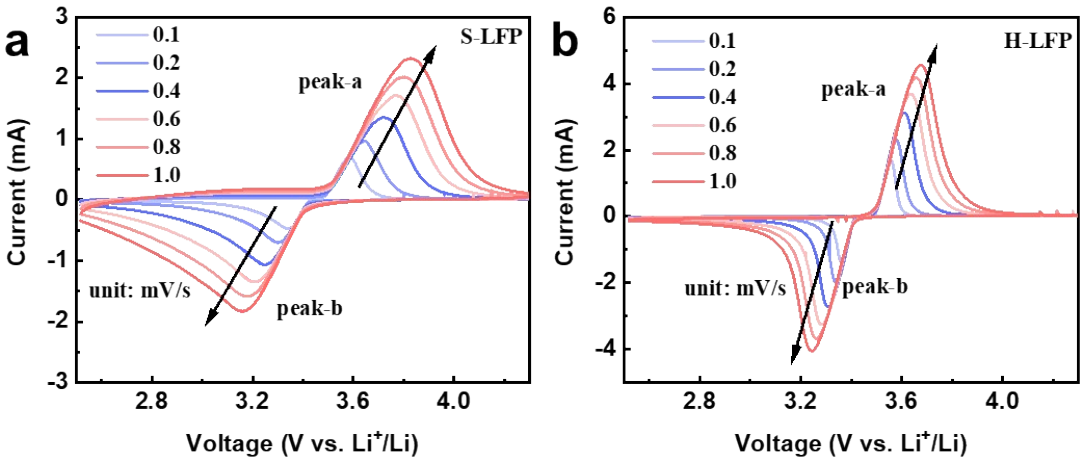

Fig. S11 CV curves of S-LFP (a) and H-LFP (b) at different sweep speeds.

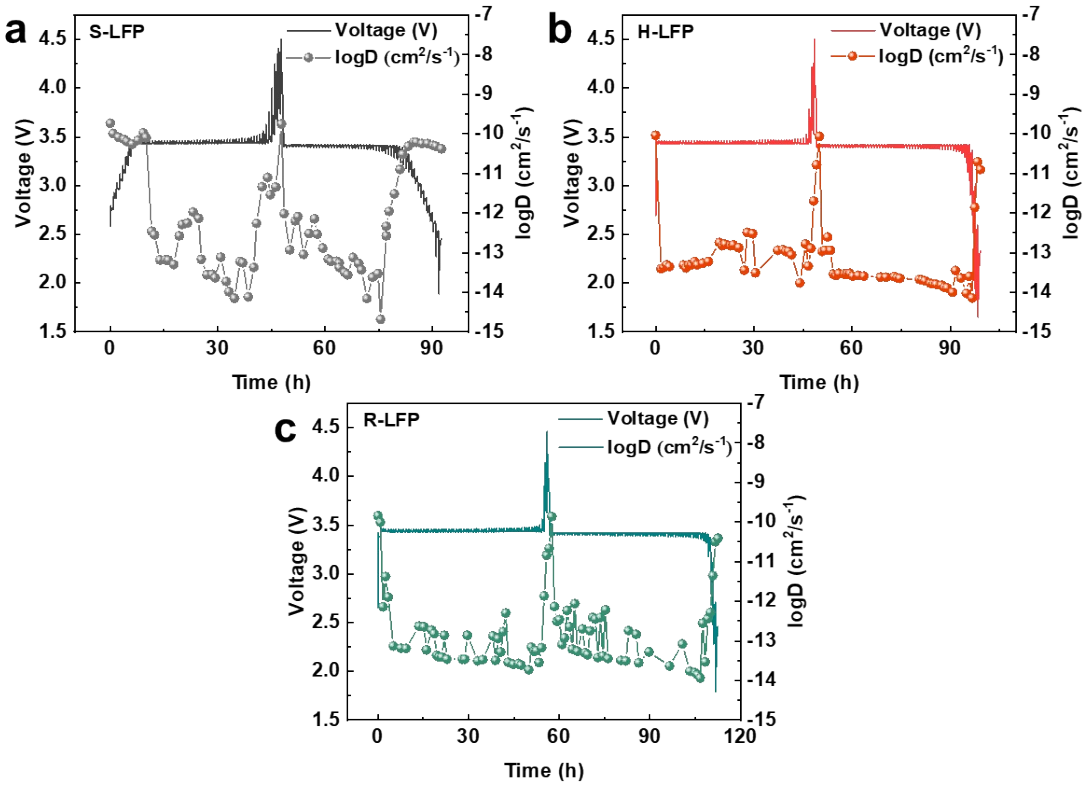

Fig. S12 GITT profiles for the discharge/charge process and diffusion coefficients of S-LFP (a), H-LFP (b) and (c) R-LFP.

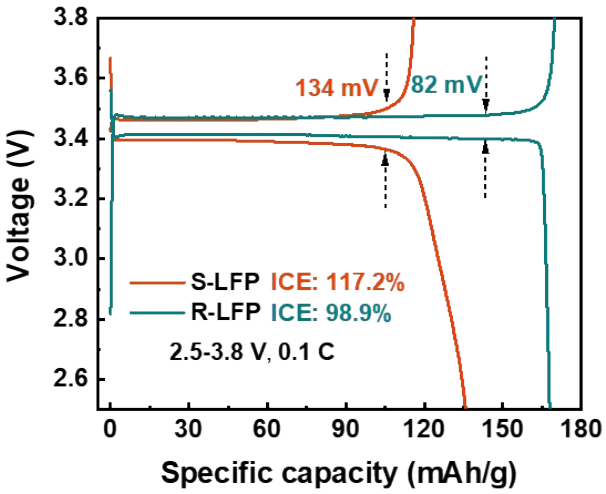

Fig. S13 The initial charge and discharge curves of S-LFP and R-LFP at 0.1 C.

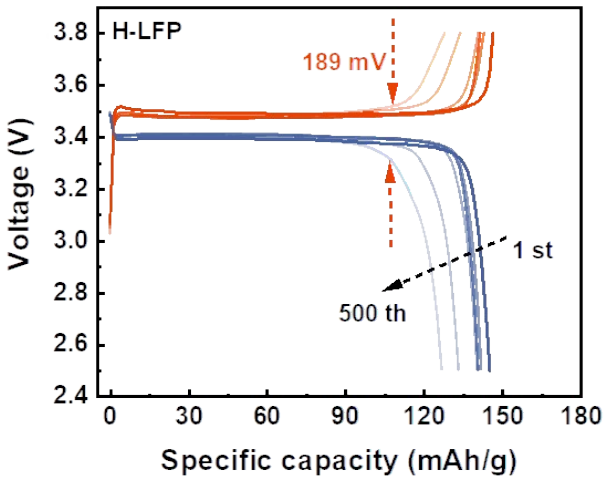

Fig. S14 Charge/discharge curves of H-LFP at various number of cycles.

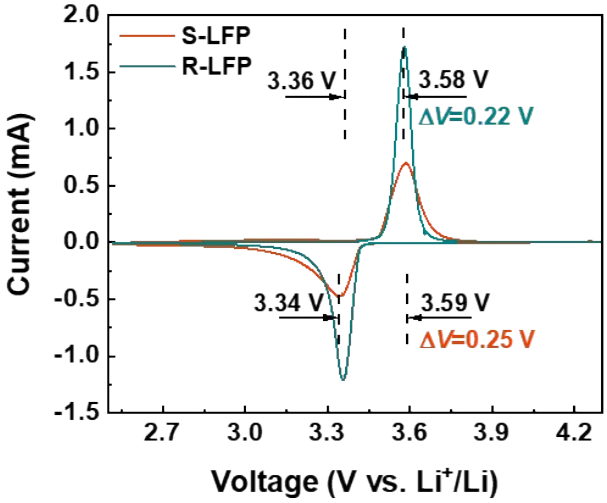

Fig. S15 CV curves at a scanning rate of 0.1 mV/s of S-LFP and R-LFP.

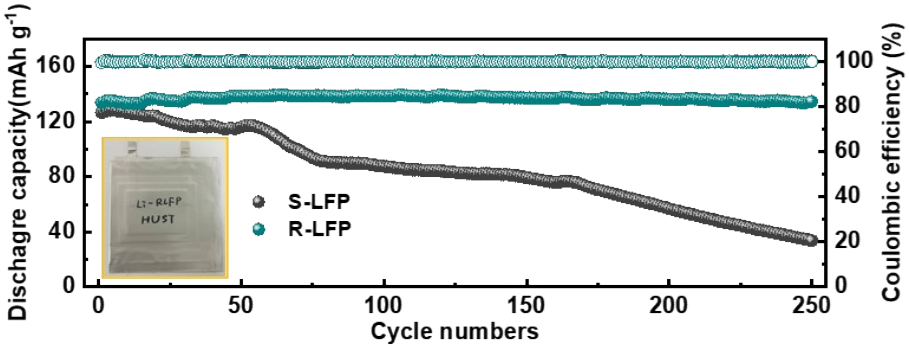

Fig. S16 Cycling performances of $LiFePO_4$||Li pouch cells of S-LFP and R-LFP.

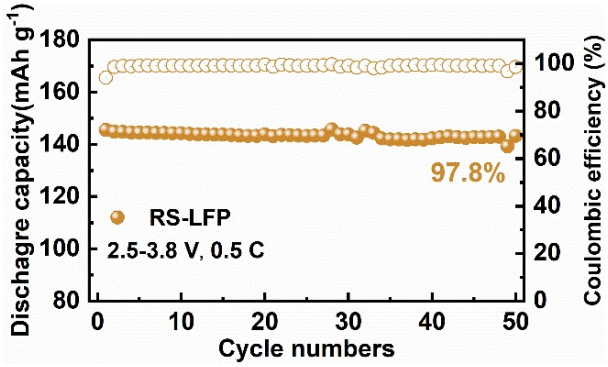

Fig. S17 Cycling performances of RS-LFP.

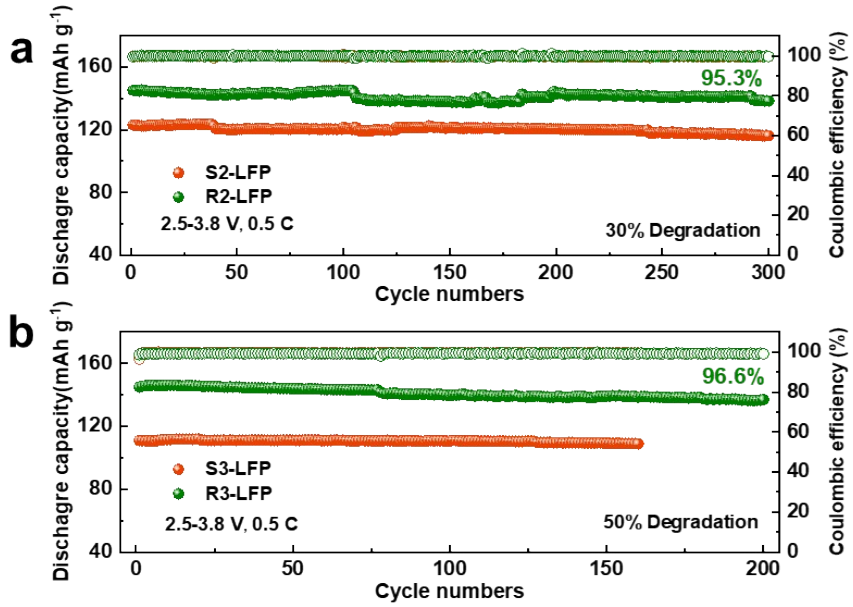

Fig. S18 Cycling performances of S2-LFP, R2-LFP, S3-LFP and R3-LFP with different degradation.

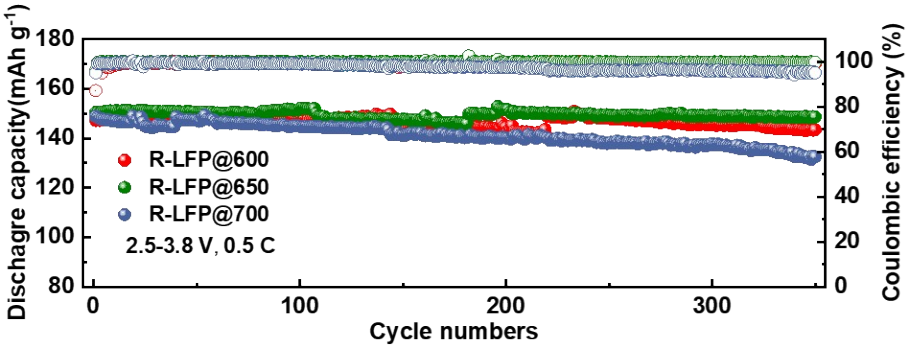

Fig. S19 Cycling performances of R-LFP obtained at different annealing temperatures.

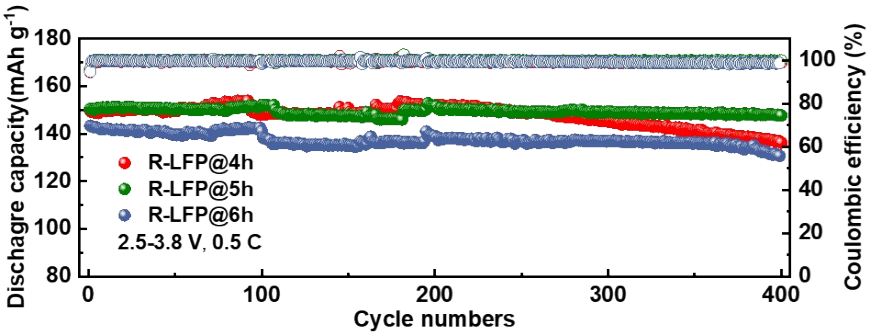

Fig. S20 Cycling performances of R-LFP obtained at different annealing times.

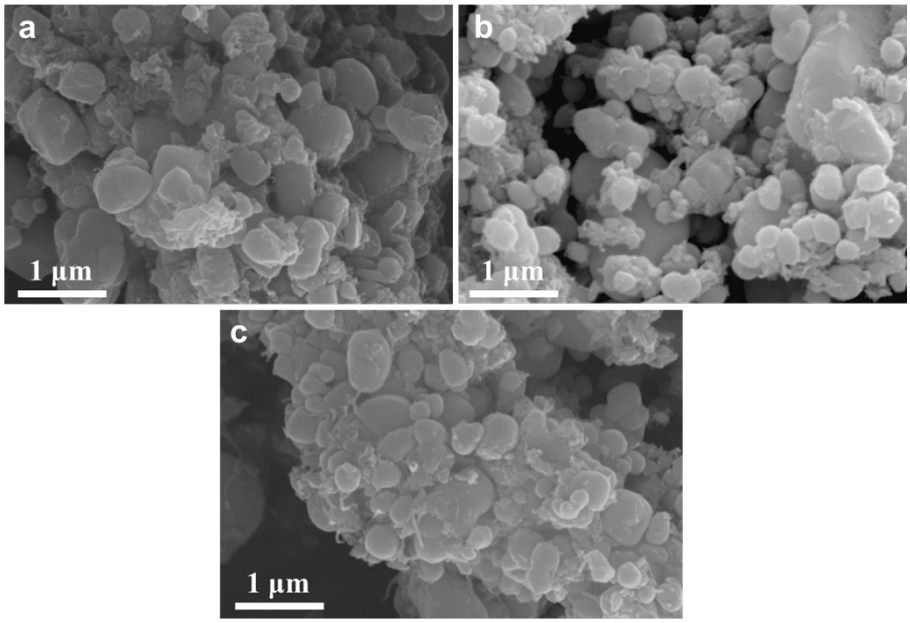

Fig. S21 SEM images of R-LFP obtained at different annealing temperatures.

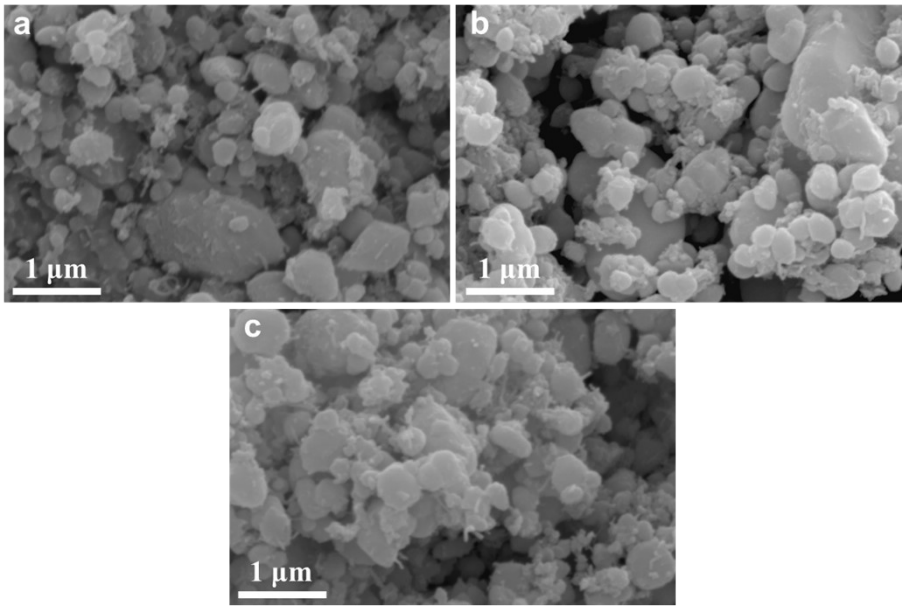

Fig. S22 SEM images of R-LFP obtained at different annealing times.

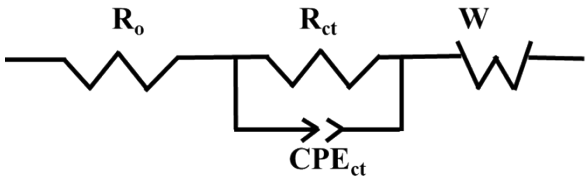

Fig. S23 Equivalent circuit model used to fit experimental EIS data.

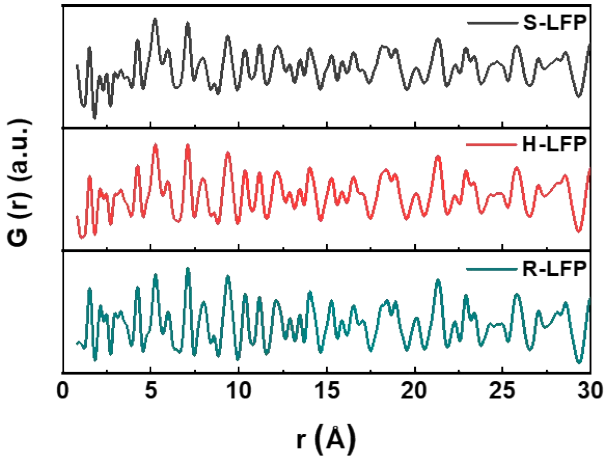

Fig. S24 Neutron PDF data of S-LFP, H-LFP, and R-LFP with the data range from 0.8 to 30 Å.

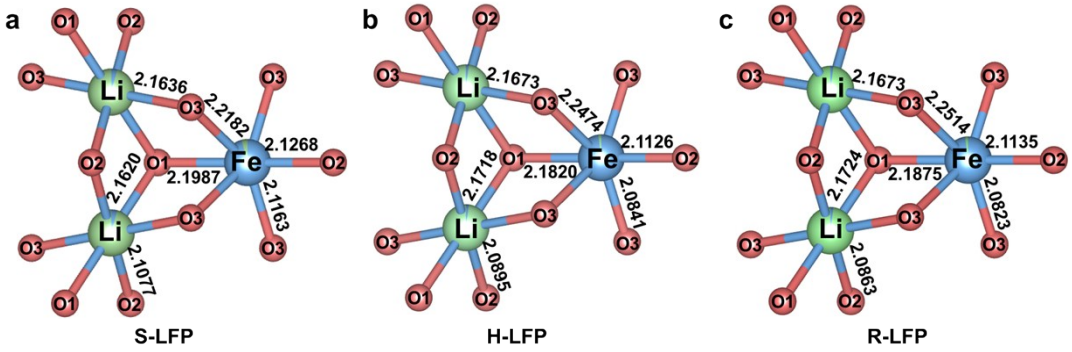

Fig. S25 Bond lengths of S-LFP, H-LFP and R-LFP.

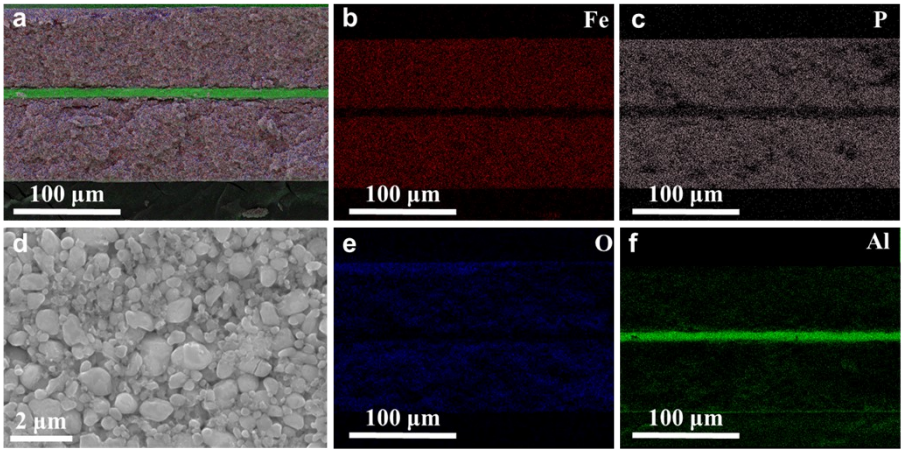

Fig. S26 SEM and EDS images of S-LFP cathode (Fe, P, O and Al elements).

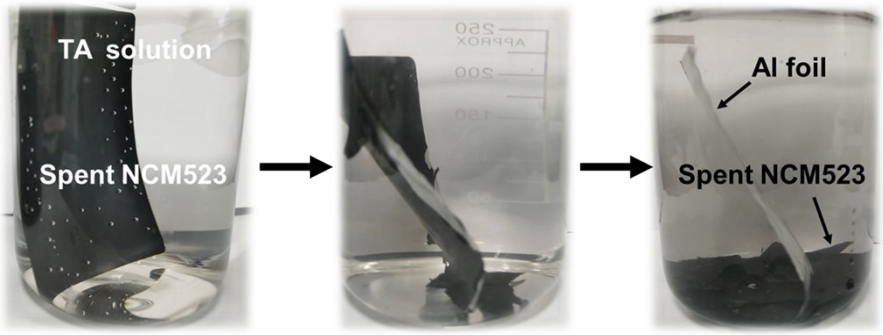

Fig. S27 Separation process of Al foil with spent NCM523 cathode material

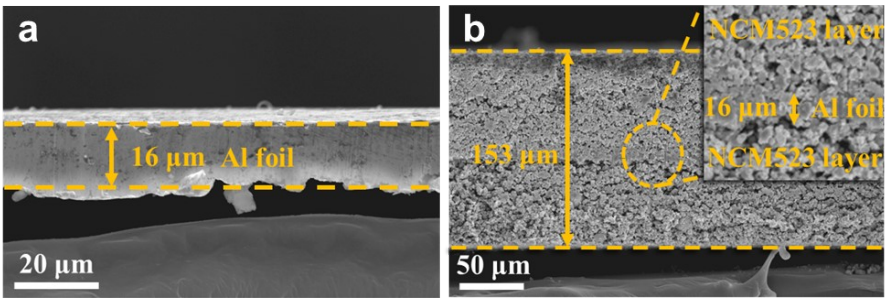

Fig. S28 SEM images for (a) separated foil and (b) spent NCM523 cathode.

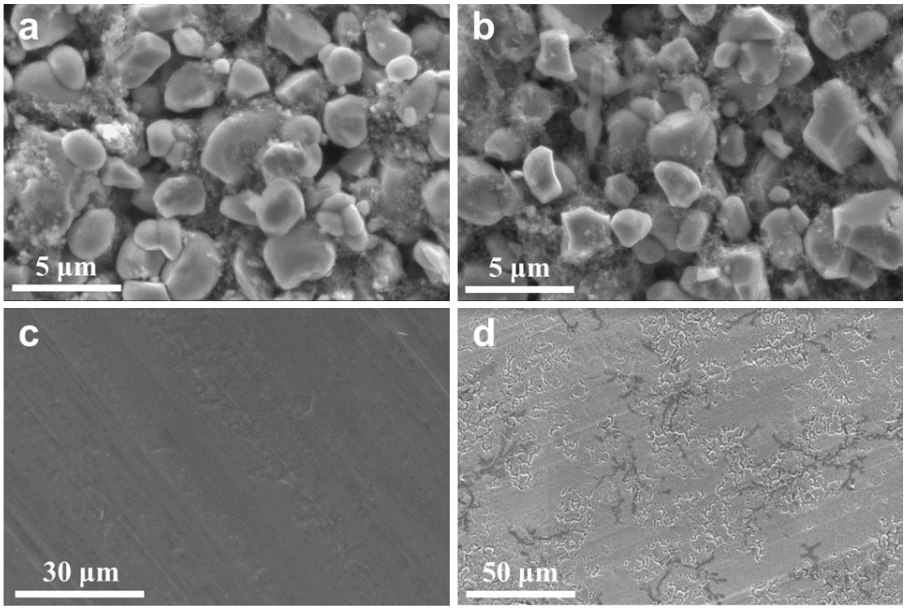

Fig. S29 (a, b) SEM images of spent NCM523 before and after separation with TA solution. (c, d) SEM images of Al foil before and after separation with TA solution.

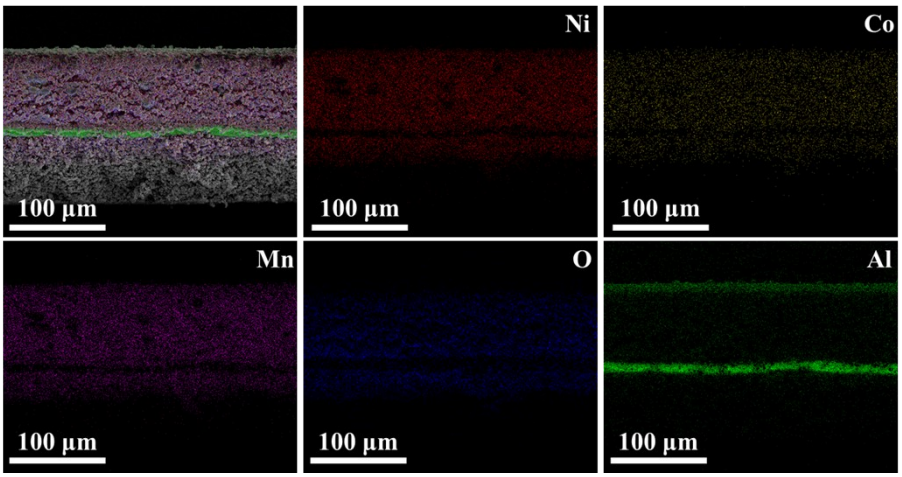

Fig. S30 EDS image of spent NCM523 cathode (Ni, Co, Mn, O and Al elements).

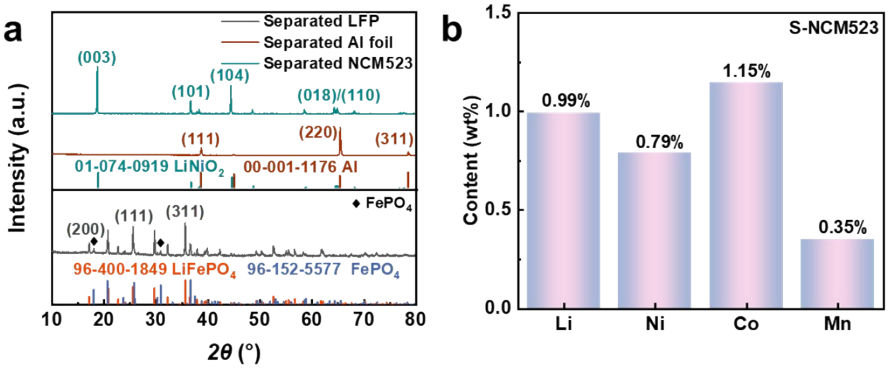

Fig. S31 (a) XRD patterns of separated Al foil, spent NCM523 and spent LFP. (b) Content of Li, Ni, Co and Mn in TA solution after separation of spent NCM523.

Table S1. Elemental analysis of S-LFP under different hydrothermal conditions.

	Element contents (ppm)			Molar ratio of
	Li 670.783	**Fe 238.204**	**P 214.914**	**Li/Fe**
S-LFP	3.08	30.67	17.15	0.8080
100-5h	2.73	24.73	13.81	0.8883
110-5h	2.48	20.57	11.42	0.9701
120-5h	3.06	24.46	13.64	1.0066
130-5h	2.35	19.17	10.64	0.9864
150-5h	1.95	16.48	9.15	0.9521
120-3h	3.41	31.18	17.35	0.8800
120-4h	2.97	25.23	13.89	0.9472
120-5h	3.06	24.46	13.64	1.0066
120-6h	3.01	24.37	13.52	0.9938
0.50	2.58	24.31	13.89	0.8540
0.75	2.79	24.17	13.45	0.9288
1.00	3.06	24.46	13.64	1.0066
1.25	2.89	23.39	12.85	0.9942

Table S2. Elemental analysis of S-LFP, H-LFP, R-LFP and C-LFP.

	Element contents (ppm)			Molar ratio of
	Li 670.783	**Fe 238.204**	**P 214.914**	**Li/Fe**
S-LFP	3.08	30.67	17.15	0.8080
H-LFP	3.06	24.46	13.64	1.0066
R-LFP	3.26	25.31	14.17	1.0364
C-LFP	4.35	33.54	18.74	1.0436

Table S3. Elemental analysis of S2-LFP, S3-LFP, S4-LFP, R2-LFP, R3-LFP and R4-LFP.

	Element contents (ppm)			Molar ratio of
	Li 670.783	**Fe 238.204**	**P 214.914**	**Li/Fe**
S2-LFP	2.43	27.50	15.32	0.7110
S3-LFP	1.48	23.62	13.07	0.5042
S4-LFP	0.46	14.88	8.19	0.2487
R2-LFP	3.81	29.63	16.24	1.0347
R3-LFP	3.42	26.84	14.87	1.0253
R4-LFP	3.26	25.62	14.26	1.0239

Table S4. Fitting result of an equivalent circuit model for impedance parameters at different states of S-LFP. (C-charge; D-discharge)

SOC/DOD	R_o (Ω)	R_{ct} (Ω)
C-3.2	8.23	83.72
C-3.3	7.5	76.47
C-3.4	7.8	79.64
C-3.5	5.88	70.63
C-3.6	4.31	52.3
C-4.0	4.703	51.08
C-4.3	4.008	49.55
D-4.0	4.704	42.21
D-3.6	4.713	33.1
D-3.5	4.766	34.17
D-3.4	5.476	37.51
D-3.3	5.383	44.77
D-3.2	5.633	83.72

Table S5. Fitting result of an equivalent circuit model for impedance parameters at different states of H-LFP. (C-charge; D-discharge)

SOC/DOD	R_o (Ω)	R_{ct} (Ω)
C-3.2	6.515	60.21
C-3.3	6.443	59.35
C-3.4	6.542	61.89
C-3.5	6.519	58.73
C-3.6	6.328	53.45
C-4.0	6.175	49.51
C-4.3	6.185	49.3
D-4.0	3.567	21.89
D-3.6	3.476	21.23
D-3.5	3.644	23.99
D-3.4	3.907	30.28
D-3.3	3.622	26.74
D-3.2	3.689	28.14

Table 6. Fitting result of an equivalent circuit model for impedance parameters at different states of R-LFP. (C-charge; D-discharge)

SOC/DOD	R_o (Ω)	R_{ct} (Ω)
C-3.2	4.479	23.88
C-3.3	4.488	24.06
C-3.4	4.588	25.32
C-3.5	4.583	25.59
C-3.6	4.397	22.96
C-4.0	4.431	20.09
C-4.3	4.441	20.12
D-4.0	4.207	9.137
D-3.6	4.21	9.613
D-3.5	4.427	11.47
D-3.4	4.851	15.15
D-3.3	4.544	13.32
D-3.2	4.583	14.46

Table S7. Structural parameters obtained from Rietveld refinement of XRD diffraction pattern of S-LFP. Phase 1 $LiFePO_4$: Space group: Pnma, R_{wp} = 2.12%, a = 10.31611 Å, b=6.001 Å, c=4.6895 Å, α = β = γ = 90°.Fraction: 81.8%。Phase 2 $FePO_4$: Space group: Pnma, a = 9.8094 Å, b = 5.7862 Å, c = 4.7799 Å, α = β = γ = 90°, Fraction: 18.2%

$LiFePO_4$ (81.8%)					
Atoms	**Site**	**Wyckoff positions**			**Occupancy**
Fe1	4c	0.28300	0.25	0.97376	0.966
Fe2	4a	0	0	0	0.034
Li1	4a	0	0	0	0.966
Li2	4c	0.28300	0.25	0.97376	0.034
P1	4c	0.09697	0.25	0.42041	1
O1	4c	0.09314	0.25	0.74072	1
O2	4c	0.45749	0.25	0.19651	1
O3	8d	0.16440	0.04698	0.28142	1

$FePO_4$ (18.2%)					
Atoms	**Site**	**Wyckoff positions**			**Occupancy**
Fe1	4c	0.27598	0.25	0.95906	0.986
P1	4c	0.09560	0.25	0.39755	1
O1	4c	0.13418	0.25	0.74837	1
O2	4c	0.46834	0.25	0.12921	1
O3	8d	0.17642	0.02646	0.24853	1

Table S8. Structural parameters obtained from Rietveld refinement of XRD diffraction pattern of H-LFP. $LiFePO_4$: Space group: Pnma, R_{wp} = 2.10%, a = 10.32133 Å, b = 6.00284 Å, c = 4.68877 Å, α = β = γ = 90°.

Atoms	**Site**	**Wyckoff positions**			**Occupancy**
Fe1	4c	0.28203	0.25	0.97425	0.98
Fe2	4a	0	0	0	0.02
Li1	4a	0	0	0	0.98
Li2	4c	0.28203	0.25	0.97425	0.02
P1	4c	0.09495	0.25	0.42083	1
O1	4c	0.09481	0.25	0.74867	1
O2	4c	0.45417	0.25	0.20945	1
O3	8d	0.16292	0.042083	0.28389	1

Table S9. Structural parameters obtained from Rietveld refinement of XRD diffraction pattern of R-LFP. $LiFePO_4$: Space group: Pnma, R_{wp} = 2.08%, a = 10.32554 Å, b = 6.00472 Å, c = 4.69001 Å, α = β = γ = 90°.

Atoms	Site	Wyckoff positions			Occupancy
Fe1	4c	0.28217	0.25	0.9734	0.982
Fe2	4a	0	0	0	0.018
Li1	4a	0	0	0	0.982
Li2	4c	0.28217	0.25	0.9734	0.018
P1	4c	0.09472	0.25	0.42372	1
O1	4c	0.09548	0.25	0.7529	1
O2	4c	0.45313	0.25	0.21807	1
O3	8d	0.16352	0.04802	0.28312	1

Table S10. Structural parameters obtained from Rietveld refinement of the neutron diffraction pattern of S-LFP. Phase 1 $LiFePO_4$: Space group: Pnma, R_{wp} = 2.62%, a = 10.3428 Å, b = 6.0164 Å, c = 4.7022 Å, α = β = γ = 90°.Fraction: 82.9% 。 Phase 2 $FePO_4$: Space group: Pnma, a = 9.8390 Å, b = 5.7998 Å, c = 4.7954 Å, α = β = γ = 90°, Fraction: 17.1%

$LiFePO_4$ (82.9%)

Atoms	Site	Wyckoff positions			Occupancy
Fe1	4c	0.28235	0.25	0.97014	0.968
Fe2	4a	0	0	0	0.032
Li1	4a	0	0	0	0.968
Li2	4c	0.28235	0.25	0.97014	0.032
P1	4c	0.09495	0.25	0.41411	1
O1	4c	0.09585	0.25	0.74575	1
O2	4c	0.45980	0.25	0.19869	1
O3	8d	0.16494	0.05357	0.27458	1

$FePO_4$ (17.1%)

Atoms	Site	Wyckoff positions			Occupancy
Fe1	4c	0.26684	0.25	0.96559	0.968
P1	4c	0.09045	0.25	0.43416	1
O1	4c	0.11666	0.25	0.77404	1
O2	4c	0.44956	0.25	0.13784	1
O3	8d	0.16978	0.07897	0.27367	1

Table S11. Structural parameters obtained from Rietveld refinement of neutron diffraction pattern of H-LFP. $LiFePO_4$: Space group: Pnma, R_{wp} = 2.56%, a = 10.3187 Å, b = 6.0022 Å, c = 4.6928 Å, α = β = γ = 90°.

Atoms	Site	Wyckoff positions			Occupancy
Fe1	4c	0.28233	0.25	0.97314	0.979
Fe2	4a	0	0	0	0.021
Li1	4a	0	0	0	0.979
Li2	4c	0.28233	0.25	0.97314	0.021
P1	4c	0.09385	0.25	0.41601	1
O1	4c	0.09821	0.25	0.74447	1
O2	4c	0.45803	0.25	0.20422	1
O3	8d	0.16373	0.04948	0.28227	1

Table S12. Structural parameters obtained from Rietveld refinement of neutron diffraction pattern of R-LFP. $LiFePO_4$: Space group: Pnma, R_{wp} = 4.96%, a = 10.3288 Å, b = 6.0059 Å, c = 4.69043 Å, α = β = γ = 90°.

Atoms	Site	Wyckoff positions			Occupancy
Fe1	4c	0.28246	0.25	0.9745	0.985
Fe2	4a	0	0	0	0.015
Li1	4a	0	0	0	0.985
Li2	4c	0.2824	0.25	0.9745	0.015
P1	4c	0.0935	0.25	0.4147	1
O1	4c	0.0982	0.25	0.7447	1
O2	4c	0.4581	0.25	0.2054	1
O3	8d	0.1634	0.0486	0.283	1